Optical Quantum State Tomography

William Bidle*

Department of Physics & Astronomy,
Stony Brook University,
Stony Brook, NY 11794-3800,
U.S.A.

(Dated: February 1, 2023)

This paper provides an overview of the application of quantum state tomography for quantum states of light. It summarizes some of the essential concepts and applications regarding quantum state reconstruction through the experimental method of optical homodyne tomography. The technique of maximum likelihood estimation of a quantum state's density matrix is discussed, and several examples are explored.

CONTENTS

I. INTRODUCTION

The main purpose of this document is to answer the questions of "how do we experimentally measure the quantum state of light," as well as "how do we then interpret it?" It should serve as a helpful guide for those who are interested in the field of quantum information science to be able to conceptually understand the underlying quantum theory, as well as replicate the process experimentally.

Many applications of quantum information applied to optical systems rely on the polarization state of light to encode information. While this serves a very practical purpose [15, 12], it turns out to be difficult to retrieve that information as we go down to the single photon level, an essential tool needed for the field of quantum information science. A superconducting nanowire single-photon detector (SNSPD) does the trick for single photon detection, however in many real world cases, we are dealing with several photon states,[1] and an SNSPD tells us nothing about the information that was encoded. Additionally, any important information that may have been encoded in the phase of the photon would be lost, since again, SNSPD's can only tell you that a photon is there.

The basic idea behind Quantum State Tomography (QST) is that for a set of measured statistical values of an identically prepared quantum state, we are able deduce a best possible guess for what that quantum state is. The idea is not too dissimilar from a CT scan of the brain, where several different 2D snapshots of the brain are layered together in order to create an accurate 3D rendering of what is actually going on, as seen in Fig. 1.

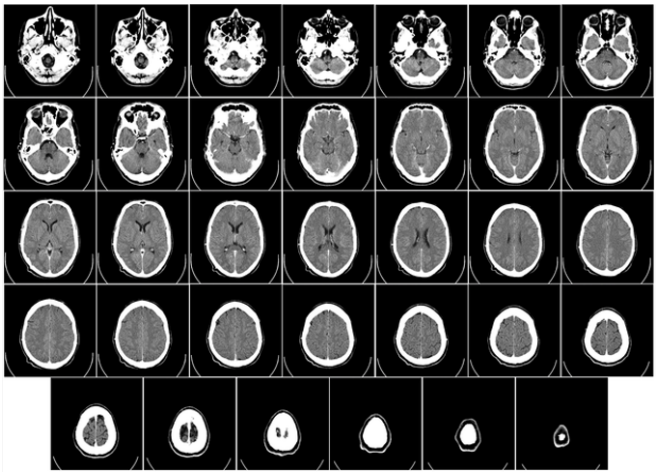

FIG. 1 CT scan of the human brain. Several different 2D snapshots are taken at different heights to put together a full 3D picture. [Image Source]

* william.bidle@stonybrook.edu

[1] As of the writing of this document, there is no such thing as a true single photon source. As a cheap (but no so great) alternative, many fall back on using weakly attenuated coherent states to simulate a single photon source. For some insight into more research being done on single photon sources, see [4] and [5].

This will obviously be much more difficult in the quantum world, as we will be dealing with quantum phase-space as opposed to a physical 3D space, but the idea is still the same. In the next section, we will start to lay down some of the necessary theoretical background before diving into the weeds of developing an algorithm to determine the most likely quantum state for a given set of "projections."

II. THEORETICAL BACKGROUND

A. Second Quantization

Before we can even start to discuss measuring single level photon states with a detector, we must first discuss what photons are, and how we can measure them in a continuous space (i.e., their electric field amplitudes). Since a photo detector essentially makes measurements of a light source's electric field, our goal here is to determine a quantum operator that represents the electric field of a photon. In the absence of any sources,[2] Maxwell's equations yield a vector potential given by an expansion of plane waves:[3]

$$\boldsymbol{A}(\boldsymbol{r},t)=\sum_{\alpha,\boldsymbol{k}}\epsilon_{\alpha,k}(A_{\alpha,k}e^{i(\boldsymbol{k}\cdot\boldsymbol{r}-\omega t)}+A^*_{\alpha,k}e^{-i(\boldsymbol{k}\cdot\boldsymbol{r}-\omega t)}) \quad (1)$$

where the sum is over the different polarizations, α, as well as the different electric field modes, $\boldsymbol{k}$. If we restrict ourselves to a box of volume $V=L^3$, the total energy of the radiation field is given by integrating the Hamiltonian density over V with periodic boundary conditions:

$$H=\sum_{\alpha,k}\epsilon_0 V\omega_k^2[A^*_{\alpha,k}A_{\alpha,k}+A^*_{\alpha,k}A_{\alpha,k}] \quad (2)$$

It is here where we can notice a striking similarity to that of the Hamiltonian of a harmonic oscillator:

$$\hat{H}_{HO}=\frac{1}{2}\sum_k\hbar\omega(\hat{a}_k\hat{a}_k^\dagger+\hat{a}_k^\dagger\hat{a}_k) \quad (3)$$

where $\hat{a}_k^\dagger$ and $\hat{a}_k^\dagger$ are the bosonic creation and annihilation operators, respectively, such that:

$$|n_1,n_2,n_3,\ldots,n_k\rangle=\prod_k\frac{(\hat{a}_k^\dagger)^{n_k}}{\sqrt{n_k!}}|0\rangle \quad (4a)$$

and

$$[\hat{a}_i^\dagger,\hat{a}_j^\dagger]=\delta_{ij} \quad (4b)$$

with the $|n_k\rangle$ states representing the so-called "number states," also known as *Fock States* that satisfy the time-independant Schrödinger equation, $\hat{H}_{HO}|n\rangle=E_n|n\rangle$, with energy eigenvalues E_n given by:

$$E_n=\hbar\omega(n+\frac{1}{2}) \quad (5)$$

Given the similarities between Eqs. (2) and (3), we are led to make the substitutions:

$$A_k\rightarrow\sqrt{\frac{\hbar}{\omega\epsilon_0 V}}\hat{a}_k \quad (6a)$$

and

$$A_k^*\rightarrow\sqrt{\frac{\hbar}{\omega\epsilon_0 V}}\hat{a}_k^\dagger \quad (6b)$$

into Eq. (2), which leads us to the general electromagnetic field Hamiltonian:

$$\hat{H}_{EM}=\sum_{\alpha,k}\hbar\omega_k(\hat{a}_k^\dagger\hat{a}_k+\frac{1}{2}) \quad (7)$$

This is a good point to stop and reflect upon our result, as we have come to a pretty remarkable conclusion: *the electric and magnetic field components of a photon can be viewed similarly to that of the position and momentum of quantum harmonic oscillator*. Thus, in a similar fashion to the harmonic oscillator we introduce a pair of operators, $\hat{E}$ and $\hat{B}$, called the *quadratures*, which in this case represent the real and complex vibrational amplitudes of the electromagnetic oscillator, respectively [9].[4] The quadrature eigenstates, denoted $|E\rangle$ and $|B\rangle$, satisfy the eigenvalue equations $\hat{E}|E\rangle=E|E\rangle$ and $\hat{B}|B\rangle=B|B\rangle$, respectively. In terms of the familiar raising and lowering operators, the quadratures are given by:

$$\hat{E}=2^{-1/2}(\hat{A}^\dagger-\hat{A}) \quad (8a)$$

and

$$\hat{B}=i2^{-1/2}(\hat{A}^\dagger+\hat{A}) \quad (8b)$$

[2] Otherwise known as the Coulomb gauge, with $\boldsymbol{\nabla}\cdot\boldsymbol{A}=0$

[3] I will be working in SI units throughout the rest of this document

[4] The typical notation that is used in the literature is $\hat{q}$ and $\hat{p}$, but I think this can confuse the reader into thinking we are dealing with non-photonic systems, such as the harmonic oscillator described in the text. If you ever get confused, just remember that $\hat{q}\leftrightarrow\hat{B}$ and $\hat{p}\leftrightarrow\hat{E}$. Regardless, it is important to know that the quadratures represent the electric and magnetic field amplitudes of the photon.

While the quadrature states themselves are not very useful, they play an important role in helping to define the so-called *quadrature wavefunctions* $\psi_n(E) = \langle n|E\rangle$ and $\psi_n(B) = \langle n|B\rangle$, which turn out to be very useful:

$$\psi_n(E) = \langle n|E\rangle = \left(\frac{1}{\pi}\right)^{1/4} \frac{H_n(E)}{\sqrt{2^n n!}} e^{-\frac{E^2}{2}} \tag{9a}$$

and

$$\psi_n(B) = \langle n|B\rangle = \left(\frac{1}{\pi}\right)^{1/4} \frac{H_n(B)}{\sqrt{2^n n!}} e^{-\frac{B^2}{2}} \tag{9b}$$

where H_n denotes the n^{th} Hermite polynomial. The states given in Eq. (9a) and (9b) represent projections of a Fock state onto the continuous basis of the photon's electric and magnetic fields, respectively. This becomes extremely useful when we actually look to measure quantum states of light in the lab (see Sec. II.B). Again, it is important to realize the major distinction between Eqs. (9a) and (9b) in the case of a harmonic oscillator and in the case of a photon - in the former's case, we are dealing with the oscillator's position and momentum, whereas in the latter's case we are looking at the photon's electric and magnetic fields amplitudes. Examples of some of the states described by in Eq. (9a)/(9b) as well as the corresponding probability distributions[5] can be seen in Fig. (2a) and (2b), respectively.

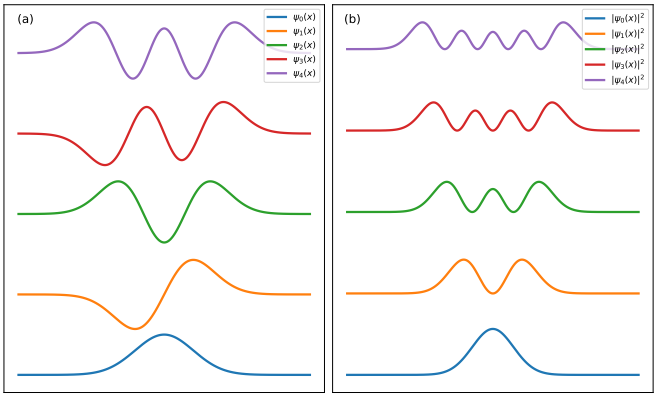

FIG. 2 Examples of (a) the lowest five Fock state wavefunctions, given by Eq. (9a), as well as (b) their corresponding probability distributions.

B. Measuring Quantum States with a Photodetector

Now what about real world measurements? When we go to measure a single photon source, for example, how do we know we are looking at single photons and not more? How confident can we be that the state we are observing is not something else (see Sec. II.C for an illustrative example)? Before tackling these questions, we should remind ourselves of how optical states are measured in the lab with photodetectors. Since the output voltage of a photodetector measures the intensity of the incoming light field, this ultimately means that we are making a measurement of the electric field of the light source:

$$V_{det} \propto I = \frac{cn\epsilon_0}{2}|E|^2 \tag{10}$$

where c is the speed of light, n is the refractive index, and ϵ_0 is the permittivity of space. We already figured out what the non-classical electric field distributions should look like for quantum states, as per Eq. (9a), but what will this look like on our photodetector? As we know, quantum states are probabilistic in nature [6], which therefore requires us to make many measurements of identically prepared systems to build up the full picture of our quantum state in question. Much like when determining the probabilities of classical events, such as whether or not a coin is "weighted," it is never enough to just measure once.[6] Therefore by sampling the same quantum system many times under identical circumstances, we can recover probability distributions similar to those shown in Fig. (3).

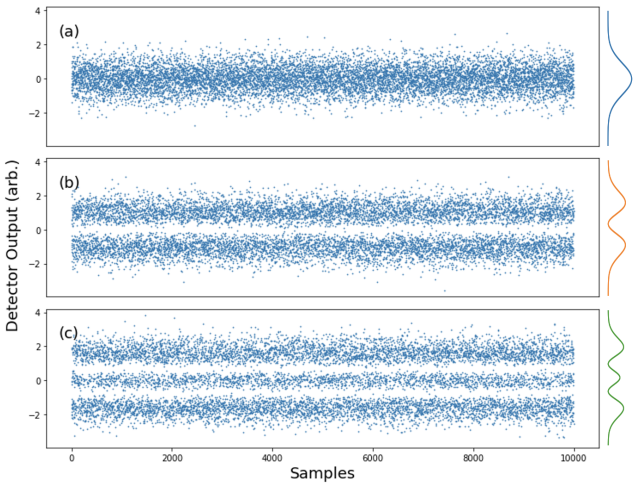

FIG. 3 Examples of the theoretical statistical measurements of the quantum states (a) $|0\rangle$, (b) $|1\rangle$, and (c) $|2\rangle$ as measured by a photo detector.

[5] $|\psi|^2$

[6] Or even a few times, for that matter.

C. Quantum Phase Space and the Wigner Distribution

Now in principle, one might think that Eq. (9a) is all that is needed to be able to extract information about a quantum state. As shown in the drawings to the right of each statistical dataset in Fig. (3), we can hypothetically recover the exact quantum state in question by fitting Eq. (9a) to the statistical data (an example of doing this with experimental data can be seen in Section III).

There are two problems with this approach, however. The first is that we are almost never dealing with pure states in the real world[7]. Since there are no reliable single photon sources as of yet, any quantum state produced in the lab will be some linear combination of different Fock states. Each of these states will therefore have it's own complex component of electric and magnetic field, contributing to the overall wavefunctions in Eq. (9a). This actually turns out to be the least of our problems, as modern day computers can generally handle complex fitting problems pretty well.[8]

The second, more problematic issue is that, in principle, two quantum states could look identical when measured by a photodetector. As an illustrative example, consider the two states $|\psi_1\rangle = \frac{1}{\sqrt{2}}(|0\rangle + i|1\rangle)$ and $|\psi_2\rangle = \frac{1}{\sqrt{2}}(|0\rangle - i|1\rangle)$ whose statistical distributions are given by Figs. (4a) and (4b), respectively. If we tried to just fit these two states to the functions given in Eq. (9a), we would not be able to recover the complex phase element that sets the two states apart from one another. The two states are completely indistinguishable, and valuable information stored in the phase of the quantum state is lost!

In order to solve this problem, we need to change our perspective in quantum phase space. The idea is actually inspired from the medical practice of a CT scan. By taking many different 2D projections of the complex 3D brain, we can accurately determine the brain's shape and structure with accuracy. A visual example of this can be seen in Fig. 5 for a complex 3D shape. The only way to properly determine the shape with absolute certainty is to look at every 2D projection from all angles.

Due to our need to probe the quantum state in phase-space, it would be convenient to work within some sort of phase-space framework. It is here where we can introduce the all important Wigner function [14, 9]:

$$W(x,p) = \frac{1}{\pi\hbar}\int_{-\infty}^{\infty}\langle x-y|\hat{\rho}|x+y\rangle e^{-2ipy/\hbar}\,dy \qquad (11)$$

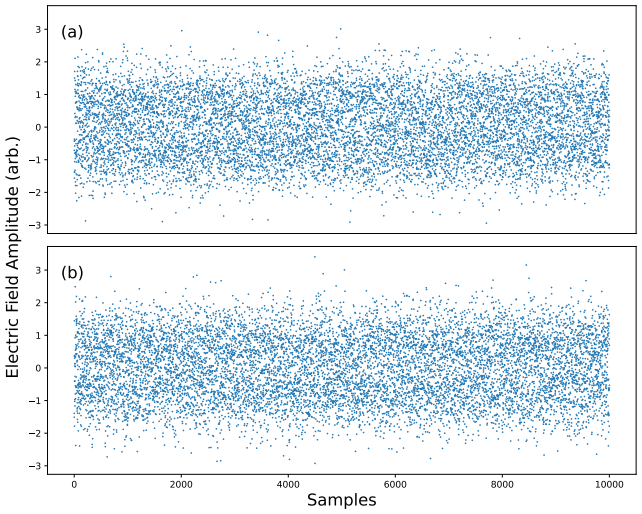

FIG. 4 Simulated detector measurements of (a) $|\psi_1\rangle = \frac{1}{\sqrt{2}}(|0\rangle + i|1\rangle)$ and (b) $|\psi_2\rangle = \frac{1}{\sqrt{2}}(|0\rangle - i|1\rangle)$ according to Eqs. (9a) and (10) over 10,000 sample statistical measurements. Notice how the two are practically indistinguishable despite being different quantum states. In this case, the relative information stored in the phase of the "qubits" is lost.

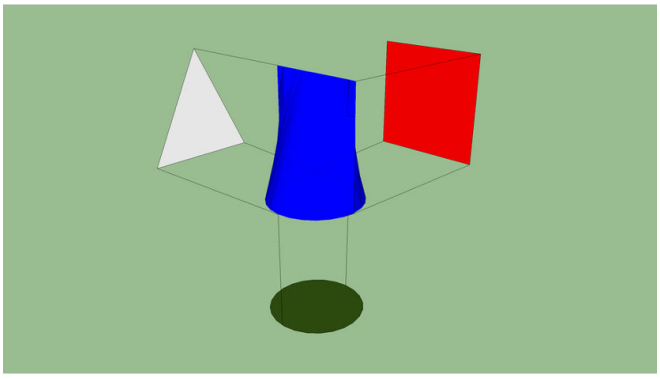

FIG. 5 Different 2D projections of a complex 3D shape. In order to properly determine the actual 3D shape, many different 2D projections need to be analyzed from many different angles. [Image Source]

where $\hat{\rho} = \sum_m \sum_n \rho_{mn}|m\rangle\langle n|$ is the quantum state's density matrix in the Fock basis. The idea is to map the density operator of the quantum state to a phase-space. Some examples of Wigner Distributions can be seen in Fig. (6). Notice how the function goes negative for some of the states, as is allowed by Eq. (11), and is therefore referred to as a quasi-probability distribution.

One of the most important features of the Wigner distribution is that it will always be unique for a given quantum state [9]. That is, *no two unique quantum states will produce the same Wigner function.* This has huge implications for being able to distinguish different quantum states, and may potentially save us from our problematic example as given by Fig. (3). Let's now look at

[7] The exception to this is the vacuum state, $|0\rangle$, however this obviously has no real interest in quantum information processing on it's own.

[8] That is, assuming the state space under consideration is small and finite.

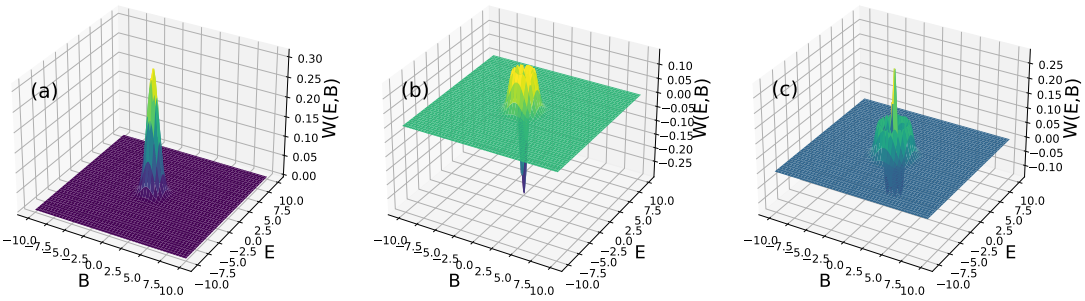

FIG. 6 Example Wigner distributions, W(E,B) in the E and B phase space of photons for the states (a) $|0\rangle$, (b) $|1\rangle$, and (c) $|2\rangle$. Notice how the Wigner distribution for the $|1\rangle$, and $|2\rangle$ states goes negative for certain values of E and B, while the $|0\rangle$ state is strictly positive - in fact, it is just a simple Gaussian.

what these states look like in phase-space, as seen in Fig. (7). Several different angles are provided to illustrate the similarities and differences in the two states depending on how they are viewed.

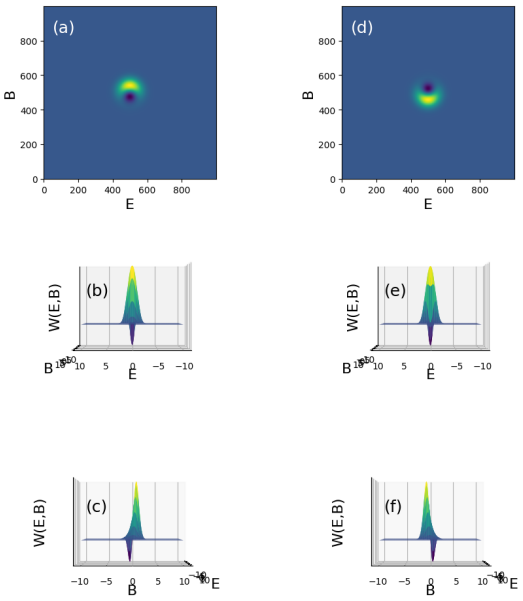

FIG. 7 Different angles of the Wigner distribution for the states (a-c) $|\psi_1\rangle = \frac{1}{\sqrt{2}}(|0\rangle + i|1\rangle)$ and (d-f) $|\psi_2\rangle = \frac{1}{\sqrt{2}}(|0\rangle - i|1\rangle)$. Notice how the two states look identical when projected along the electric field axis, but their differences are revealed when we look at the different projections along the magnetic field axis. This then suggests that we need to find a way to view the quantum state from different angles in phase-space.

From a top view, as in Figs. (7a) and (7d), it is clear that the Wigner distribution of the two states are different. However, as we have already seen, if the two states are looked at purely along the electric field axis, as in Figs. (7b) and (7e), they appear to be identical. If we change our perspective by 90 degrees to look along the magnetic field axis, the differences of the two states are revealed. This then suggests that if we were to somehow rotate ourselves or the quantum state in phase-space, we would be able to reveal their differences. If we were able to accomplish this, then in essence, we could fit the Wigner distribution of the quantum state in question to completely characterize it's properties, and the problem presented in Fig. (4) would vanish. So the question then is: "how we can change our perspective in quantum phase-space to make these differences more apparent, while still performing measurements on a photodetector (i.e., still looking at the electric field projection)?"

The answer lies in interferometry.[9] By interfering the same signal with itself after one of the arms has had it's path length changed, we can simulate the effect of rotating the quantum state in phase space. In effect, this allows us to see into different projections of the quantum state while still only looking along it's electric field projection. The greater the phase difference between the two arms, the more in phase-space we will rotate.[10] Experimentally, we can accomplish this effect with an optical homodyne detector, which will be explored more in Sec. III.

Mathematically, if we introduce the phase shift operator given by:

$$\hat{U}(\theta) = e^{i\theta\hat{n}} \tag{12}$$

and apply this to a random Fock state $|\psi\rangle = |n\rangle$, we find that:

$$\hat{U}(\theta)|\psi\rangle = e^{i\theta\hat{n}}|n\rangle = e^{in\theta}|n\rangle \tag{13}$$

[9] In fact, almost any situation involving phase will point to interferometry.

[10] That is up until $\theta = 2\pi$.

where I have used the tricks that $e^{i\theta\hat{n}} = \sum_{k=0}^{\infty} \frac{(i\theta\hat{n})^k}{k!}$ and $\hat{n}|n\rangle = n|n\rangle$. It is here where we can now find the modified versions of Eqs. (9a) and (9b) with the addition of the phase term from Eq. (13):

$$\psi_n(\theta, E) = \langle n|\theta, E\rangle = e^{in\theta} \left(\frac{1}{\pi}\right)^{1/4} \frac{H_n(E)}{\sqrt{2^n n!}} e^{-\frac{E^2}{2}} \quad (14a)$$

and

$$\psi_n(\theta, B) = \langle n|\theta, B\rangle = e^{in\theta} \left(\frac{1}{\pi}\right)^{1/4} \frac{H_n(B)}{\sqrt{2^n n!}} e^{-\frac{B^2}{2}} \quad (14b)$$

One thing we can immediately notice is that the new phase term in Eqs. (14a) and (14b) will only affect the anti-diagonal terms of a quantum state, providing us with a way to probe the different components of the state. If we now look at the statistical distribution of the two problematic states considered in Fig. 4, but now using Eq. (14a) to generate the statistics as a function of the phase, θ, we can easily distinguish the two, as seen in Fig. 8.

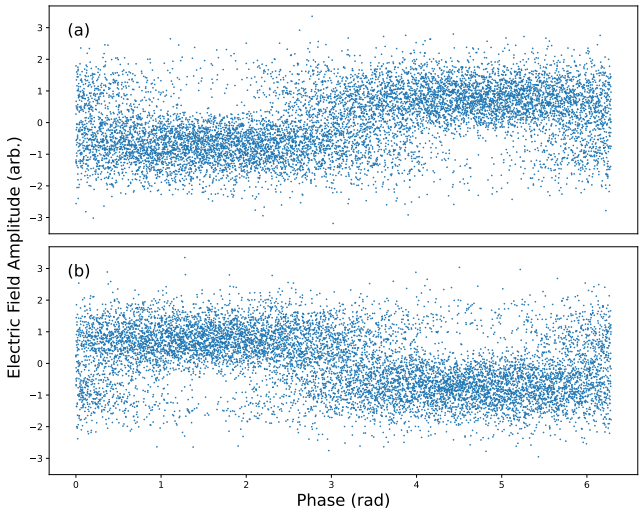

FIG. 8 Statistical measurements of (a) $|\psi_1\rangle = \frac{1}{\sqrt{2}}(|0\rangle + i|1\rangle)$ and (b) $|\psi_2\rangle = \frac{1}{\sqrt{2}}(|0\rangle - i|1\rangle)$ according to Eq. (14a). Notice how now the two states can be easily distinguished.

Since we are able to look at the two states from many different angles, their differences suddenly become apparent, and we can now recover information that was once lost. A visual example of this process can be seen in Fig. (8), which shows the evolution of the state in Fig. (7) in phase-space. As the state is rotated in phase-space, the electric field projection changes and allows us to probe the full picture of the quantum state.

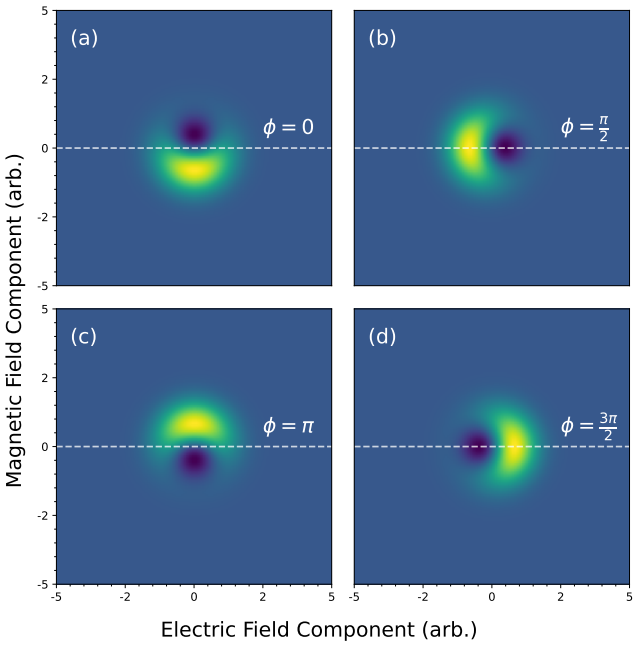

FIG. 9 Evolution of the quantum state from Fig. 7(a) in the phase-space described by Eq. 11 for phase values of (a) 0, (b) $\frac{\pi}{2}$, (c) π, and (d) $\frac{3\pi}{2}$. The white horizontal dotted line in each image is an example of the state's projection as viewed from the E-field axis.

D. Coherent States

One of the more important optical quantum states that shows up in almost every experimental setting is the coherent state $|\alpha|$, which accurately describes the behavior of in-phase laser light. A coherent state satisfies the eigenvalue equation $\hat{a}|\alpha\rangle = \alpha|\alpha\rangle$. The raising operator is not Hermitian, therefore α is not always real, and can be written in a complex form as $\alpha = |\alpha|e^{i\theta}$, where $|\alpha|$ is the coherent state amplitude, and θ is the phase. This form is convenient for representing the state in phase space. In the Fock state representation, a coherent state is given by:

$$|\alpha\rangle = e^{-\frac{|\alpha|^2}{2}} \sum_{n=0}^{\infty} \frac{\alpha^n}{\sqrt{n!}} |n\rangle \quad (15)$$

An example of the quadrature statistics as a function of phase can be seen in Fig. 9 for $\alpha = \sqrt{10}$.

III. HOMODYNE TOMOGRAPHY

I will now focus on some details of how to implement the ideas in the previous section into real world practice. As mentioned, in order to accomplish the phase-space probing of our quantum states that we desire, we need to turn to interferometry. More specifically, we need to

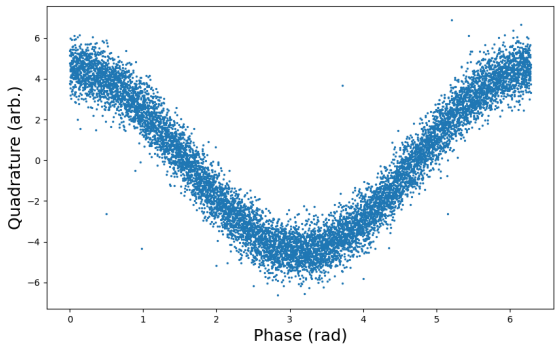

FIG. 10 Example of the quadrature statistics of a coherent state with $\alpha = \sqrt{10}$.

use a homodyne detector, which is an extremely useful device for measuring the phase-sensitive properties of a light field [3, 9].

When applied to quantum optics, a homodyne detector will directly measure phase dependent quadrature values of a quantum state's electric field. The basic schematic for performing homodyne detection of a quantum state can be seen in Fig (11). Two input fields, denoted the local oscillator (LO) and probe are incident on a 50/50 beam splitter (BS) and the two outputs are passed through a balanced photo detector.

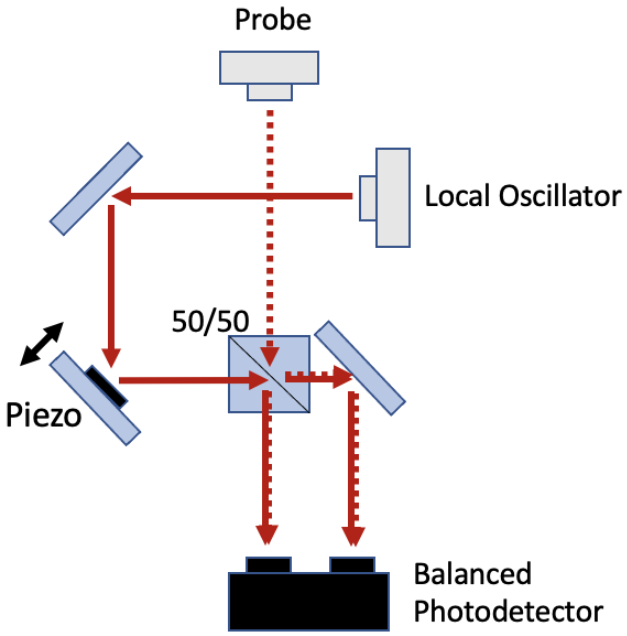

FIG. 11 Schematic for a basic optical homodyne detector. Two input fields, denoted the local oscillator and probe are incident on a 50/50 beam splitter and the two outputs are passed through a balanced photo detector.

Since a photodetector will make a measurement proportional to the intensity of the light field, as given by Eq. (10), we can write the output voltage of the balanced photodetector as;

$$V_{homo} = (\hat{E}_{Probe} + \hat{E}_{LO})^2 - (\hat{E}_{Probe} - \hat{E}_{LO})^2 \quad (16)$$

An example of measuring a vacuum state with a homodyne detector can be seen in Fig. (12).[11]. Quadrature statistics of the state's electric field were measured as the LO phase was scanned and the probe output was blocked. The measured quadratures were then binned into histograms and fit to the vacuum wavefunction, $\psi_0(E)$, as given in Eq. 9a to determine the so-called "vacuum width" that is necessary for re-scaling any subsequent data.

IV. MAXIMUM LIKELIHOOD RECONSTRUCTION

Since any quantum state can be written as a superposition of Fock states, we can therefore write the wavefunction as a linear combination of states given in Eq. (14a) and (14b) for any photon number. If we were to know the quantum state in advance, we would therefore be able to easily predict the quadrature statistics that the state would produce on a photodetector. Examples of this were shown in Sec. II.C for the states $|\psi_1\rangle = \frac{1}{\sqrt{2}}(|0\rangle + i|1\rangle)$ and $|\psi_2\rangle = \frac{1}{\sqrt{2}}(|0\rangle - i|1\rangle)$, which can both be written in quadrature space as $\langle\psi_1|\theta, E\rangle = (\frac{2}{\pi})^{1/4}\frac{1}{\sqrt{2}}e^{-E^2}(1 + ie^{i\theta}\sqrt{2}E)$ and $\langle\psi_2|\theta, E\rangle = (\frac{2}{\pi})^{1/4}\frac{1}{\sqrt{2}}e^{-E^2}(1 - ie^{i\theta}\sqrt{2}E)$, respectively. From here, probabilistic sampling can be done as a function of the phase, θ, which again, was explained in Sec. II.C.

In reality, however, we won't know in advance what our quantum state is, and we are therefore tasked with the reverse problem - given a set of experimental quadrature data, we need to determine what the corresponding quantum state is. This is obviously a much more difficult problem and may not be as easy as a simple fitting exercise, especially when the possible state space under consideration can be infinite.

There are two main reconstruction methods that are typically used to reconstruct a quantum state through OHT. The first is a so-called "inverse linear transform" technique, which relies on the fact that Eq. (11) can be inverted due to the linear properties of integrals [11]. A more common approach relies of statistical inference, and more specifically, maximum likelihood estimation (MLE) of the density matrix for the measured quantum state [11]. The latter of these two will be discussed here.

[11] This data was taken with a in-house built homodyne detector in the Figueroa Lab at Stony Brook University.

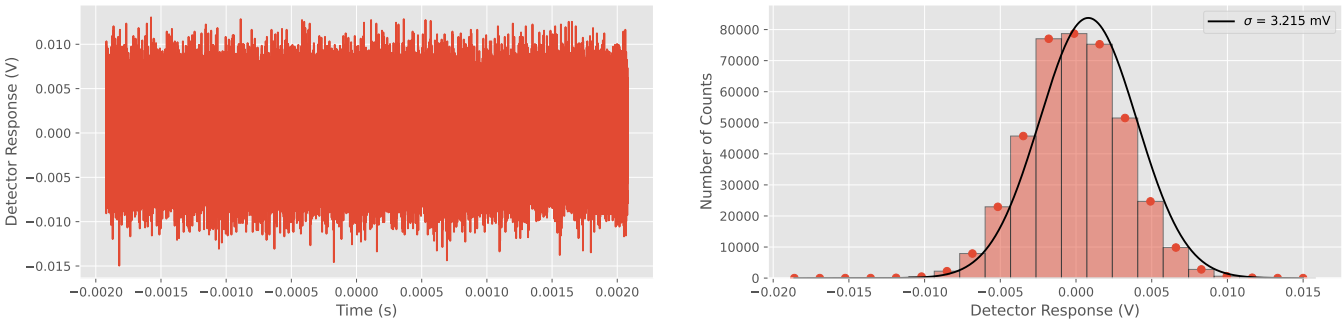

FIG. 12 (a) Real data of the vacuum state from a homodyne detector along with (b) a fit of the binned statistics in order to accurately determine the state, as outlined in Sec. II.

A. Derivation of the MLE Algorithm

The basic approach to MLE [8] is that we are hoping to find a density matrix that has the *highest probability* of representing the statistics of some measured quantum state. In other words, we are looking to maximize the likelihood that a given density matrix describes the measured quadrature data given by:

$$\mathcal{L}(\hat{\rho}) = \prod_{i=1}^{N} \mathrm{pr}(\theta_i, E_i) \tag{17a}$$

or

$$\ln[\mathcal{L}(\hat{\rho})] = \sum_{i=1}^{N} \ln[\mathrm{pr}(\theta_i, E_i)] \tag{17b}$$

where $\mathrm{pr}(\theta_i, E_i) = \langle \theta_i, E_i|\hat{\rho}|\theta_i, E_i\rangle = \mathrm{Tr}[\hat{\Pi}(\theta_i, E_i)\hat{\rho}]$ is the probability of measuring a particular quadrature value with $\hat{\Pi}(\theta_i, E_i) = |\theta_i, E_i\rangle\langle\theta_i, E_i|$ being the projection operator in the continuous quadrature space. That is, we are looking to find a density matrix that best represents the entire dataset, $\{(\theta_i, E_i)\}$. The logarithm of the likelihood (log-likelihood) is usually considered to make the proceeding approach a little more mathematically friendly. We therefore want to find a $\hat{\rho}$ that maximizes Eq. (17b) under the constraint that it's trace is equal to unity. This essentially boils down to optimizing a constrained function, $F(\hat{\rho})$, which can be done through the method of Lagrange multipliers:

$$F(\hat{\rho}) = \ln[\mathcal{L}(\hat{\rho})] + \lambda\Phi(\hat{\rho}) \tag{18}$$

where $\Phi(\hat{\rho}) = \mathrm{Tr}[\hat{\rho}] = 1$ is the constraint and λ is the Lagrange multiplier. Our goal is to first find what λ is. We can start by realizing that when we are at a maximum, Eq. (18) will be zero:

$$\frac{dF}{d\hat{\rho}} = \frac{d\ln[\mathcal{L}(\hat{\rho})]}{d\hat{\rho}} + \lambda\frac{d\Phi}{d\hat{\rho}} = \frac{d}{d\hat{\rho}}\left[\ln[\mathcal{L}(\hat{\rho})] + \lambda\mathrm{Tr}[\hat{\rho}]\right] = 0 \tag{19}$$

In other words, making small changes to the density matrix will not change the constrained function. Substituting in the definition of $\ln[\mathcal{L}(\hat{\rho})]$ from Eq. (17b):

$$\sum_{i=1}^{N} \frac{1}{\mathrm{pr}(\theta_i, x_i)} \frac{d}{d\hat{\rho}}(\mathrm{Tr}[\hat{\Pi}(\theta_i, x_i)\hat{\rho}]) = -\lambda\frac{d}{d\hat{\rho}}(Tr[\hat{\rho}]) \tag{20}$$

If we now utilize the fact that $\frac{d}{d\hat{B}}\mathrm{Tr}[\hat{A}\hat{B}] = \hat{A}^T$, $\frac{d}{d\hat{B}}\mathrm{Tr}[\hat{B}] = \hat{\mathbb{1}}$, and $|\theta_i, x_i\rangle\langle\theta_i, x_i| = |\theta_i, x_i\rangle\langle\theta_i, x_i|^T$, then we find that

$$\sum_{i=1}^{N} \frac{1}{\mathrm{pr}(\theta_i, x_i)}|\theta_i, x_i\rangle\langle\theta_i, x_i| = -\lambda\hat{\mathbb{1}} \tag{21}$$

We can then multiply both sides by $\hat{\rho}$:

$$\sum_{i=1}^{N} \frac{1}{\mathrm{pr}(\theta_i, x_i)}|\theta_i, x_i\rangle\langle\theta_i, x_i|\hat{\rho} = -\lambda\hat{\rho} \tag{22}$$

and take the trace of both sides to find λ:

$$\lambda = -\sum_{i=1}^{N} = -N \tag{23}$$

If we then plug this result back into Eq. (22) we then discover that:

$$\left[\frac{1}{N}\sum_{i=1} \frac{|\theta_i, x_i\rangle\langle\theta_i, x_i|}{\mathrm{pr}(\theta_i, x_i)}\right]\hat{\rho} \equiv \hat{R}(\hat{\rho})\hat{\rho} = \hat{\rho} \tag{24}$$

where we have defined the so-called "iteration operator," $\hat{R}(\hat{\rho})$. If a given density matrix $\hat{\rho}_0$ maximizes Eq. (17b), then $\hat{R}(\hat{\rho}_0) \propto \mathbb{1}$ and therefore $\hat{R}(\hat{\rho}_0)\hat{\rho}_0 = \hat{\rho}_0\hat{R}(\hat{\rho}_0) \propto \hat{\rho}_0$, as well as $\hat{R}(\hat{\rho}_0)\hat{\rho}_0\hat{R}(\hat{\rho}_0) \propto \hat{\rho}_0$. This last relation is especially useful since it returns positive diagonal elements [10, 7]. Now if a given density matrix

$\hat{\rho} \neq \hat{\rho}_0$ does not maximize Eq. (17b), then applying the operation above will result in a new density matrix that is closer to the maximum likelihood. We can therefore construct an iterative algorithm for finding the most likely density matrix:

$$\hat{\rho}^{(k+1)} = \mathcal{N}\left[\hat{R}(\hat{\rho}^k)\hat{\rho}^k\hat{R}(\hat{\rho}^k)\right] \tag{25}$$

where $\mathcal{N}$ ensures that the trace of the new density matrix is equal to unity. Following this iterative procedure, we then have a way to determine a density matrix that best matches the given quadrature statistics. Each subsequent iteration will serve to increase the likelihood of Eq. (17b). This method is very similar to the technique of gradient descent, visually demonstrated by Fig. 13.

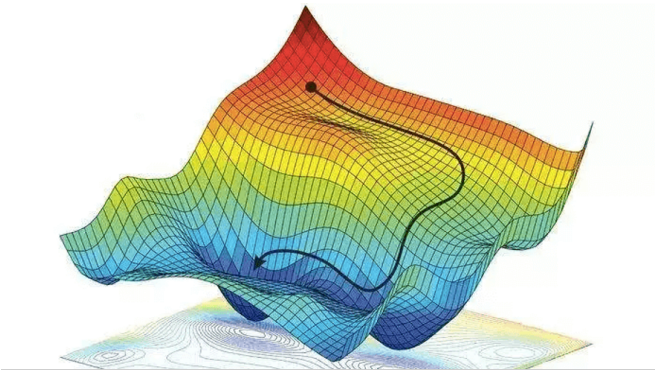

FIG. 13 Visualization of the method of gradient descent on a complex 3D landscape. The technique of MLE for QST described in the text has the potential to be an infinite dimensional landscape, so do your best to imagine that as you see fit. Image Source

Now a closer inspection of Eq. (25) will reveal that this can be a rather time-consuming problem depending on the amount of data points in the quadrature statistics, N, and dimensionality of the Fock space we wish to consider, n. Viewing the operators in Eq. (25) as matrices, $\hat{R}(\hat{\rho})$ will be of size $(N \times N)$ and $\hat{\rho}$ will be of size $(n \times n)$, leading to a computational run-time of $\mathcal{O}(N^2n^2)$. This can be an absolutely huge number for one run, even with a small number of quadrature data points ($\sim$1000) and low dimensionality of considered states ($\sim$10). In many situations within the realm of quantum information processing, it is essential to be able to determine the measured quantum state in real-time. As a classical example, you can imagine how painful it would be for it to take days before a text you sent to a friend to arrive to their phone.[12] Therefore, it becomes essential to vectorize the computational process such that density matricies can be determined in real-time. This is explained further in Sec. V.

B. Statistical Uncertainty

Before I show off some examples of this powerful technique, it is first important to discuss how we can statistical uncertainties that arise in our results. Since we are unable to consider the full, infinite-dimensional space spanned by our state, we will naturally be missing some key information that allows us to precisely pin down the quantum state we are dealing with.[13] Additionally, in a typical experiment we only sample with a subset of quadrature values for a given quantum state, and since the measurements exist within a continuous space, we naturally are only looking at a subset of the full quantum state.[14]

Therefore, it becomes an important step to understand the uncertainty in the final reconstructed density matrix. A common approach [11] to dealing with these uncertainties lies in a Monte Carlo-like simulation. We essentially look to simulate quadrature data that corresponds to our estimated density matrix, $\hat{\rho}$, which resulted from the iterative algorithm in Eq. (25), and perform MLE on the generated quadratures to get a new set of density matrices, $\{\hat{\rho}'_i\}$. The statistical uncertainty, $\delta\hat{\rho}$, in $\hat{\rho}$ is then given by the average difference between the simulated data and the actual data given by:

$$\delta\hat{\rho} = \frac{1}{N}\sum_i^N |\hat{\rho} - \hat{\rho}_i| \tag{26}$$

This method then provides us with a good idea of the statistical error of the given dataset. One very important thing to note, however, is that this will not provide information on whether or not the reconstructed state is correct or not. All Eq. (26) will tell us is the statistical uncertainty associated with the dataset, since it simulates new quadrature data based off of what we *think* the correct density matrix is. One way to test the actual accuracy of the algorithm would be to use simulated data that has a known quantum state, and see how well the algorithm can reconstruct the individual elements.

---

[12] Obviously quantum phones are not a thing of the near future (if ever), but it is fun to dream...

[13] This is especially true with coherent states.

[14] An obvious solution to this would be to just take more measurements, but as seen in the previous section, the computational complexity of the reconstruction grows with the square of the number of data points taken. If time was not a limiting factor, then this would be a good solution, however, one of the more desirable outcomes of such a process is to do this in real time (elaborate more).

C. Maximum Likelihood in Action

Now that we have developed both the MLE algorithm with Eq. (25) as well as a way to evaluate the performance of the reconstruction with Eq. (26), it's now finally time to bring it all together and look at some reconstructed density matrices! In all of the following examples, the Fock space under consideration was limited to the first 10 Fock states (except for the coherent states), 10,000 data points were used for the state's quadrature statistics over the 2π phase scanning period, and 20 iterations of Eq. (25) were used.[15]

As a nice and easy set of first examples, let's reconstruct the Fock states $|0\rangle$ and $|1\rangle$, whose quadrature distributions are given in Fig. (3a) and (3b) respectively. The diagonal components of the reconstructed density matrices can be seen in Fig. 14. As we can see, the algorithm was able to accurately pick out the correct states with high certainty from a fairly decently sized state space, and almost all of the non-relevant terms are nearly zero.

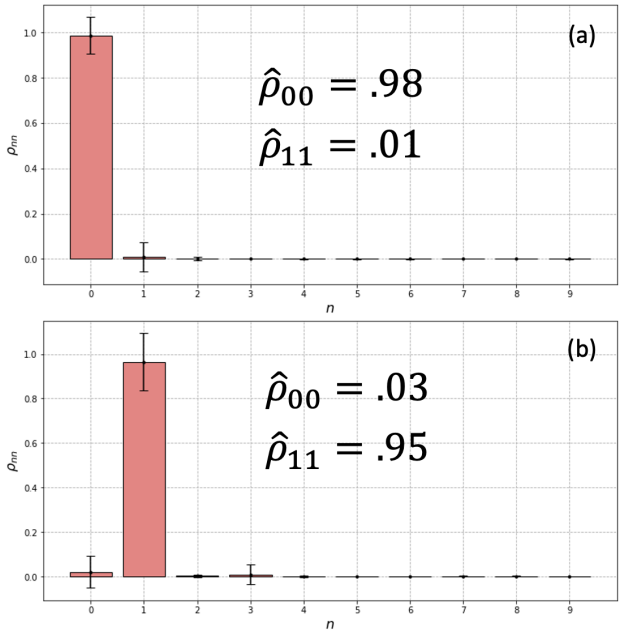

FIG. 14 First 10 diagonal components of the reconstructed density matrix for the states (a) $|0\rangle$ and (b) $|1\rangle$.

Obviously that was a fairly easy example, and we would hope that the algorithm would be able to reconstruct complex states as well. Let's now look at the reconstructed elements of the two states from Fig. (8) as seen in Fig. (14). Unlike in the previous cases, we now expect there to be non-zero diagonal elements of the density matrix, with values of $\rho_{01}(\psi_1) = -\rho_{01}(\psi_2) = 0.5i$, and $\rho_{10}(\psi_1) = -\rho_{10}(\psi_2) = -0.5i$. As we can see, these diagonal elements were almost perfectly reconstructed, and we can provide a confident answer as to what the original state in question was without having any prior information besides the quadrature statistics. Aside from a very small component of $|2\rangle$ appearing in the reconstruction,[16] the rest of the density matrix elements are again so small that they can practically be considered zero.

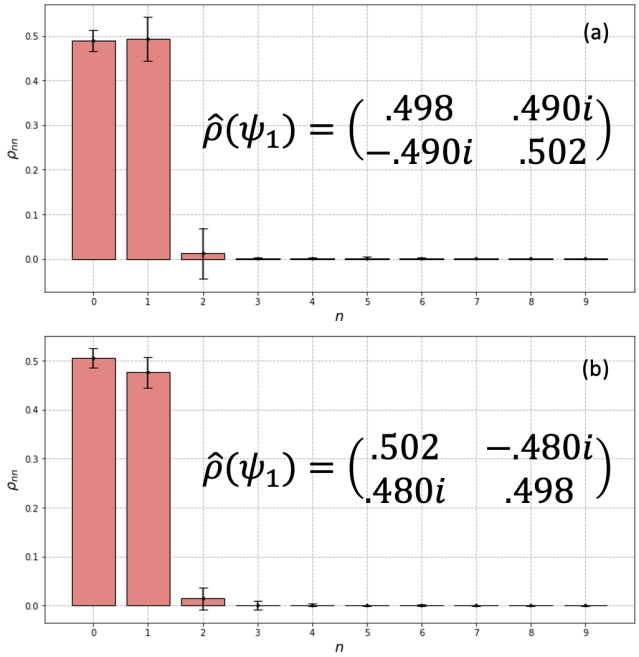

FIG. 15 First 10 diagonal components of the reconstructed density matrix for the states (a) $|\psi_1\rangle = \frac{1}{\sqrt{2}}(|0\rangle + i|1\rangle)$ and (b) $|\psi_2\rangle = \frac{1}{\sqrt{2}}(|0\rangle - i|1\rangle)$.

Finally, we can look at coherent states, which may be one of the more practical use-cases. Diagonal components of the reconstructed density matrix for simulated coherent states with average photon numbers of $n = 5.5\,(\alpha = 2.35)$ and $n = 0.8\,(\alpha = 0.89)$ can be seen in Fig. (16a) and (16b), respectively. The coherent states are then fit to Eq. (15) to try and deduce α, and therefore n. Being able to accurate determine the coefficients of the coherent state in question is essential for procedures such as quantum process tomography [13, 1].

[15] The number of iterations of the MLE algorithm is highly dependant on the number of data points used in the quadrature data. From experience, any set of quadratures with at least 1,000 data points will have convergence of Eq. (17b) for 20 iterations of Eq. (25).

[16] This is almost definitely a result of the statistical nature of quadrature sampling. If we were able to increase the number of data points considered in the simulation of these states, the small component of $|2\rangle$ would vanish much like how some of the higher order states already have.

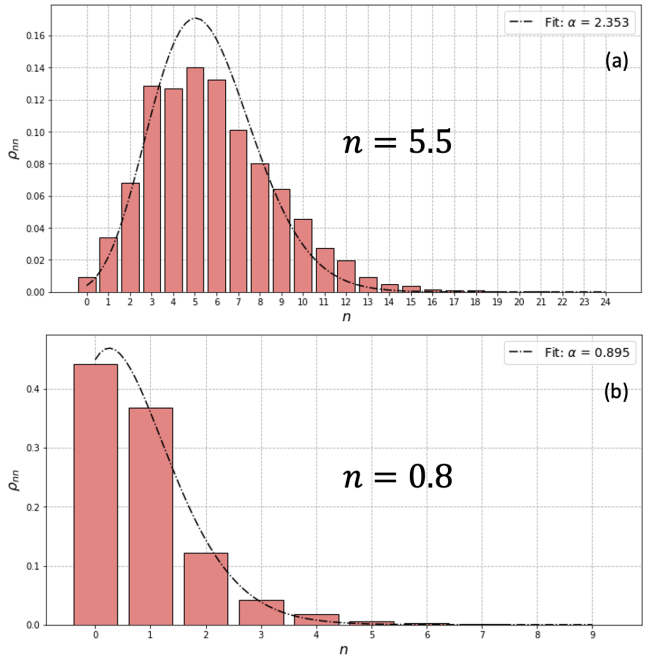

FIG. 16 Diagonal components of the reconstructed density matrix for simulated coherent states with average photon numbers of (a) $n = 5.5\,(\alpha = 2.35)$ and (b) $n = 0.8\,(\alpha = 0.89)$. The coherent states are then fit to Eq. (15) to try and deduce α, and therefore n.

V. PUBLICLY AVAILABLE CODE

In addition to this document, I have also compiled a public GitHub repository that contains all of the code as well as instructions for performing simulated QST similar to what was done throughout this document [2]. If you have any questions or find any bugs with the code, please feel free to email me at william.bidle@stonybrook.edu.

VI. ACKNOWLEDGEMENTS

There are many people who I would like to thank for helping me to compile this document. First and foremost, I would like to thank my advisor at Stony Brook, Dr. Eden Figueroa, for giving me the opportunity to work on such fascinating research. I have never met such a true visionary, and his passion for quantum information science is unmatched.

Next, I would like to thank all of the members of my research group, including but not limited to, Guo-Dong Cui, Samet Demircan, Sonali Gera, Dillion Cottrill, Chase Wallace, Anthony Del Valle, Leonardo Castillo-Veneros, and Dounan Du.

Lastly, would also like to thank all of my friends and peers at Stony Brook, primarily Aaron Mueninghoff, James Shirk, Julia Codere, Michael Ray, and Zachary Withers for their insightful discussions and support.

REFERENCES

[1] Aamir Anis and A. I. Lvovsky. "Maximum-likelihood coherent-state quantum process tomography". In: (2012). DOI: 10.48550/ARXIV.1204.5936. URL: https://arxiv.org/abs/1204.5936.

[2] William Bidle. *Quantum State Tomography*. Jan. 2023. URL: https://github.com/WilliamBidle/Quantum-State-Estimation.

[3] Samuel L. Braunstein. "Homodyne statistics". In: *Phys. Rev. A* 42 (1 July 1990), pp. 474–481. DOI: 10.1103/PhysRevA.42.474. URL: https://link.aps.org/doi/10.1103/PhysRevA.42.474.

[4] Guo-Dong Cui et al. *Coherent Quantum Interconnection between On-Demand Quantum Dot Single Photons and a Resonant Atomic Quantum Memory*. 2023. DOI: 10.48550/ARXIV.2301.10326. URL: https://arxiv.org/abs/2301.10326.

[5] Sonali Gera, Steven Sagona-Stophel, and Eden Figueroa. "MHz Source of Single Photons Tuned to Rubidium Transition". In: *OSA Quantum 2.0 Conference*. Optica Publishing Group, 2020, QTh7B.17. DOI: 10.1364/QUANTUM.2020.QTh7B.17. URL: https://opg.optica.org/abstract.cfm?URI=QUANTUM-2020-QTh7B.17.

[6] David J. Griffiths and Darrell F. Schroeter. *Introduction to quantum mechanics*. Third edition. Cambridge ; New York, NY: Cambridge University Press, 2018. ISBN: 978-1-107-18963-8.

[7] Zdeněk Hradil, Dmitri Mogilevtsev, and Jaroslav Řeháek. "Biased tomography schemes: an objective approach." In: *Physical review letters* 96 23 (2006), p. 230401.

[8] Connor Michael Kupchak. "Complete Characterization of Quantum Optical Processes with a Focus on Quantum Memory". In: (Apr. 2013). URL: https://www.iqst.ca/media/pdf/publications/ConnorKupchak.pdf.

[9] U Leonhardt. "Measuring the Quantum State of Light". In: *Measurement Science and Technology* 11.12 (Dec. 2000), p. 1827. DOI: 10.1088/0957-0233/11/12/706. URL: https://dx.doi.org/10.1088/0957-0233/11/12/706.

[10] A I Lvovsky. "Iterative maximum-likelihood reconstruction in quantum homodyne tomography". In: *Journal of Optics B: Quantum and Semiclassical Optics* 6.6 (May 2004), S556–S559. DOI: 10.1088/1464-4266/6/6/014. URL: https://doi.org/10.1088.

[11] A. I. Lvovsky and M. G. Raymer. "Continuous-variable optical quantum-state tomography". In: *Rev. Mod. Phys.* 81 (1 Mar. 2009), pp. 299–332. DOI: 10.1103/RevModPhys.81.299. URL: https://link.aps.org/doi/10.1103/RevModPhys.81.299.

[12] Cheng-Zhi Peng et al. "Experimental Long-Distance Decoy-State Quantum Key Distribution Based on Polarization Encoding". In: *Phys. Rev. Lett.* 98 (1 Jan. 2007), p. 010505. DOI: 10.1103/PhysRevLett.98.010505. URL: https://link.aps.org/doi/10.1103/PhysRevLett.98.010505.

[13] Saleh Rahimi-Keshari et al. "Quantum process tomography with coherent states". In: *New Journal of Physics* 13.1 (Jan. 2011), p. 013006. DOI: 10.1088/1367-2630/13/1/013006. URL: https://doi.org/10.1088.

[14] D. T. Smithey et al. "Measurement of the Wigner distribution and the density matrix of a light mode using optical homodyne tomography: Application to squeezed states and the vacuum". In: *Phys. Rev. Lett.* 70 (9 Mar. 1993), pp. 1244–1247. DOI: 10.1103/PhysRevLett.70.1244. URL: https://link.aps.org/doi/10.1103/PhysRevLett.70.1244.

[15] Jindong Wang et al. "Experimental demonstration of polarization encoding quantum key distribution system based on intrinsically stable polarization-modulated units". In: *Opt. Express* 24.8 (Apr. 2016), pp. 8302–8309. DOI: 10.1364/OE.24.008302. URL: https://opg.optica.org/oe/abstract.cfm?URI=oe-24-8-8302.